



HAL
open science

Untangling Local and Global Deformations in Deep Convolutional Networks for Image Classification and Sliding Window Detection

George Papandreou, Iasonas Kokkinos, Pierre-André Savalle

► **To cite this version:**

George Papandreou, Iasonas Kokkinos, Pierre-André Savalle. Untangling Local and Global Deformations in Deep Convolutional Networks for Image Classification and Sliding Window Detection. [Research Report] Toyota Technological Institute at Chicago; Ecole Centrale Paris; Inria Saclay Ile de France. 2014. hal-01109289

HAL Id: hal-01109289

<https://hal.science/hal-01109289>

Submitted on 26 Jan 2015

HAL is a multi-disciplinary open access archive for the deposit and dissemination of scientific research documents, whether they are published or not. The documents may come from teaching and research institutions in France or abroad, or from public or private research centers.

L'archive ouverte pluridisciplinaire **HAL**, est destinée au dépôt et à la diffusion de documents scientifiques de niveau recherche, publiés ou non, émanant des établissements d'enseignement et de recherche français ou étrangers, des laboratoires publics ou privés.

Untangling Local and Global Deformations in Deep Convolutional Networks for Image Classification and Sliding Window Detection

George Papandreou

Toyota Technological Institute at Chicago

gpapan@ttic.edu

Iasonas Kokkinos and Pierre-André Savalle

Ecole Centrale Paris and INRIA

[iasonas.kokkinos,pierre-andre.savalle]@ecp.fr

Abstract

Deep Convolutional Neural Networks (DCNNs) commonly use generic ‘max-pooling’ (MP) layers to extract deformation-invariant features, but we argue in favor of a more refined treatment. First, we introduce epitomic convolution as a building block alternative to the common convolution-MP cascade of DCNNs; while having identical complexity to MP, Epitomic Convolution allows for parameter sharing across different filters, resulting in faster convergence and better generalization. Second, we introduce a Multiple Instance Learning approach to explicitly accommodate global translation and scaling when training a DCNN exclusively with class labels. For this we rely on a ‘patchwork’ data structure that efficiently lays out all image scales and positions as candidates to a DCNN. Factoring global and local deformations allows a DCNN to ‘focus its resources’ on the treatment of non-rigid deformations and yields a substantial classification accuracy improvement. Third, further pursuing this idea, we develop an efficient DCNN sliding window object detector that employs explicit search over position, scale, and aspect ratio. We provide competitive image classification and localization results on the ImageNet dataset and object detection results on the Pascal VOC 2007 benchmark.

1. Introduction

Deep learning offers a powerful framework for learning increasingly complex representations for visual recognition tasks. The work of Krizhevsky et al. [18] convincingly demonstrated that deep neural networks can be very effective in classifying images in the challenging Imagenet benchmark [5], significantly outperforming computer vision systems built on top of engineered features like SIFT [22]. Their success spurred a lot of interest in the machine learning and computer vision communities. Subsequent work has improved our understanding and has refined certain aspects of this class of models [39]. A number of differ-

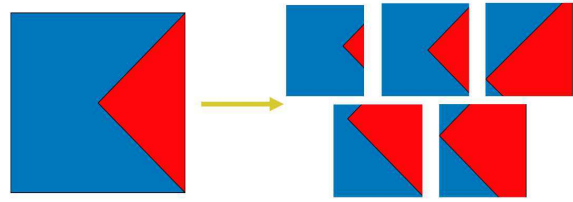


Figure 1. Epitomes represent a set of small images through a common data structure: The epitome is a single, larger image which can produce several smaller filters by picking a position and cropping a small window. While epitomes were originally employed for generative image modelling, in this work we propose to use epitomes as an efficient method for parameter sharing in Deep Learning: Epitomes are used in hierarchical networks, and their parameters are learned discriminatively through back-propagation.

ent studies have further shown that the features learned by deep neural networks are generic and can be successfully employed in a black-box fashion in other datasets or tasks such as image detection [4, 9, 26, 30, 32, 39].

The deep learning models that so far have proven most successful in image recognition tasks, e.g. [21, 33, 34], are feed-forward convolutional neural networks trained in a supervised fashion to minimize a regularized training set classification error by back-propagation. Their recent success is partly due to the availability of large annotated datasets and fast GPU computing, and partly due to some important methodological developments such as dropout regularization and rectifier linear activations [18]. However, the key building blocks of deep neural networks for images have been around for many years [19]: (1) Deep Convolutional Neural Networks (DCNNs) with small receptive fields that spatially share parameters within each layer. (2) Gradual abstraction and spatial resolution reduction after each convolutional layer as we ascend the network hierarchy, typically via max-pooling [15, 31]

This paper examines several aspects of invariance to deformations in the context of DCNNs for visual recognition. We treat both locally defined (non-rigid) and global deformations, demonstrating that a more refined treatment yields

improved classification performance.

Our first main contribution is to build a deep neural network around the epitomic representation [17]. The image epitome, illustrated in Figure 1, is a data structure appropriate for learning translation-aware image representations, naturally disentangling appearance and position modeling of visual patterns. While originally developed for generative image modelling, we show here that the epitome data structure can be used to train DCCNs discriminatively.

For this, we substitute every pair of convolution and max-pooling layers typically used in DCNNs with an ‘Epitomic Convolution’ layer. As illustrated in Fig. 2, Epitomic Convolution is an input-centered dual alternative to the filter-centered standard max-pooling. Namely, rather than searching in the input image (or layer) for the strongest response of a filter, we search across the set of filters encapsulated in a epitome for the strongest response to an image patch. Our Epitomic Convolution is designed to have the same computational and model complexity as Max-Pooling, while similar filters to share parameters.

We use a dictionary of ‘mini-epitomes’ at each network layer: each mini-epitome is only slightly larger than the corresponding input data patch, just enough to accommodate for the desired extent of position invariance. For each input data patch, the mini-epitome layer outputs a single value per mini-epitome, which is the maximum response across all filters in the mini-epitome. In [28] we discuss another deep epitomic network variant built on top of large epitomes which learns topographically organized features.

Our second main contribution is to explicitly deal with object scale and position when applying DCNNs to image classification. We show that this can be done efficiently using a patchwork data structure in a principled, consistent manner during both training and testing. While fusing classification results extracted from multiple image windows is standard practice, we show that when incorporating multiple windows during training in a Multiple Instance Learning (MIL) framework we obtain substantially larger gains.

Finally, we explore to what extent we can push scale and position search towards developing efficient and effective sliding window object detectors on top of DCNNs. We accelerate sliding window detection by introducing a simple method to reduce the effective size and receptive field of a DCNN pre-trained on ImageNet and show that by performing an explicit search over position, scale, and aspect ratios we can obtain results that are comparable to the current-state-of-the-art while being substantially simpler and easier to train, as well as more efficient.

We quantitatively evaluate the proposed models primarily in image classification experiments on the Imagenet ILSVRC-2012 large-scale image classification task. We train the model by error back-propagation to minimize the classification loss, similarly to [18]. We have experimented

with deep mini-epitomic networks of different architectures (Class A, B, and C). We have carried out the bulk of our comparisons between epitomes and max-pooling using comparable mid-sized networks having 6 convolutional and 3 fully connected layers whose structure closely follows that in [32] (Class-A). In these evaluations the deep epitomic network achieves 13.6% top-5 error on the validation set, which is 0.6% better than the corresponding conventional max-pooled convolutional network whose error rate is 14.2%, with both networks having the same computational cost. Note that the error rate of the original model in [18] is 18.2%, using however a smaller network. We have also more recently experimented with larger deep mini-epitomic networks (Class-B), which have the same number of levels but more neurons per layer than those in Class-A. The plain deep epitomic net in Class-B achieves an error rate of 11.9%. When accompanied with explicit scale and position search (patchwork variant), its error drops further down to 10.0%. Finally, following [33], we have most recently experimented with a very deep epitomic network with 13 convolutional and 3 fully connected layers (Class-C). This achieves an even lower error rate of 10.0% (without scale and position search). All these performance numbers refer to classification with a single network. We also find that the proposed epitomic model converges faster, especially when the filters in the dictionary are mean- and contrast-normalized, which is related to [39]. We have found this normalization to also accelerate convergence of standard max-pooled networks.

In [28] we further report additional sets of experiments. First, we show that a deep epitomic network trained on Imagenet can be effectively used as black-box feature extractor for tasks such as Caltech-101 image classification. Second, we report excellent image classification results on the MNIST and CIFAR-10 benchmarks with smaller deep epitomic networks trained from scratch on these small-image datasets.

Related work Our model builds on the epitomic image representation [17], which was initially geared towards image and video modeling tasks. Single-level dictionaries of image epitomes learned in an unsupervised fashion for image denoising have been explored in [1,3]. Recently, single-level mini-epitomes learned by a variant of K-means have been proposed as an alternative to SIFT for image classification [29]. To our knowledge, epitomes have not been studied before in conjunction with deep models or learned to optimize a supervised objective.

The proposed epitomic model is closely related to max-out networks [12]. Similarly to epitomic matching, the response of a maxout layer is the maximum across filter responses. The critical difference is that the epitomic layer is hard-wired to model position invariance, since filters ex-

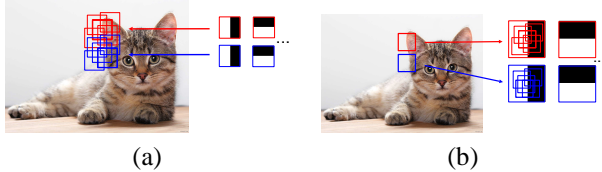


Figure 2. (a) Standard max-pooled convolution: For each filter we look for its best match within a small window in the data layer. (b) Proposed epitomic convolution (mini-epitome variant): For input data patches sparsely sampled on a regular grid we look for their best match in each mini-epitome.

tracted from an epitome share values in their area of overlap. This parameter sharing significantly reduces the number of free parameters that need to be learned. Maxout is typically used in conjunction with max-pooling [12], while epitomes fully substitute for it. Moreover, maxout requires random input perturbations with dropout during model training, otherwise it is prone to creating inactive features. On the contrary, we have found that learning deep epitomic networks does not require dropout in the convolutional layers – similarly to [18], we only use dropout regularization in the fully connected layers of our network.

Other variants of max pooling have been explored before. Stochastic pooling [38] has been proposed in conjunction with supervised learning. Probabilistic pooling [20] and deconvolutional networks [40] have been proposed before in conjunction with unsupervised learning, avoiding the theoretical and practical difficulties associated with building probabilistic models on top of max-pooling. While we do not explore it in this paper, we are also very interested in pursuing unsupervised learning methods appropriate for the deep epitomic representation.

2. Deep Epitomic Convolutional Networks

2.1. Mini-Epitomic deep networks

We first describe a single layer of the mini-epitome variant of the proposed model, with reference to Fig. 2. In standard max-pooled convolution, we have a dictionary of K filters of spatial size $W \times W$ pixels spanning C channels, which we represent as real-valued vectors $\{\mathbf{w}_k\}_{k=1}^K$ with $W \cdot W \cdot C$ elements. We apply each of them in a convolutional fashion to every $W \times W$ input patch $\{\mathbf{x}_i\}$ densely extracted from each position in the input layer which also has C channels. A reduced resolution output map is produced by computing the maximum response within a small $D \times D$ window of displacements $p \in \mathcal{N}_{input}$ around positions i in the input map which are D pixels apart from each other. The output map $\{z_{i,k}\}$ of standard max-pooled convolution has spatial resolution reduced by a factor of D across each dimension and will consist of K channels, one

for each of the K filters. Specifically:

$$(z_{i,k}, p_{i,k}) \leftarrow \max_{p \in \mathcal{N}_{image}} \mathbf{x}_{i+p}^T \mathbf{w}_k \quad (1)$$

where $p_{i,k}$ points to the input layer position where the maximum is attained (argmax).

In the proposed epitomic convolution scheme we replace the filters with larger mini-epitomes $\{\mathbf{v}_k\}_{k=1}^K$ of spatial size $V \times V$ pixels, where $V = W + D - 1$. Each mini-epitome contains D^2 filters $\{\mathbf{w}_{k,p}\}_{p \in \mathcal{N}_{epitome}}$ of size $W \times W$, one for each of the $D \times D$ displacements $p \in \mathcal{N}_{epitome}$ in the epitome. We *sparse* extract patches $\{\mathbf{x}_i\}$ from the input layer on a regular grid with stride D pixels. In the proposed epitomic convolution model we reverse the role of filters and input layer patches, computing the maximum response over epitomic positions rather than input layer positions:

$$(y_{i,k}, p_{i,k}) \leftarrow \max_{p \in \mathcal{N}_{epitome}} \mathbf{x}_i^T \mathbf{w}_{k,p} \quad (2)$$

where $p_{i,k}$ now points to the position in the epitome where the maximum is attained. Since the input position is fixed, we can think of epitomic matching as an input-centered dual alternative to the filter-centered standard max-pooling.

Computing the maximum response over filters rather than image positions resembles the maxout scheme of [12], yet in the proposed model the filters within the epitome are constrained to share values in their area of overlap.

Similarly to max-pooled convolution, the epitomic convolution output map $\{y_{i,k}\}$ has K channels and is subsampled by a factor of D across each spatial dimension. Epitomic convolution has the same computational cost as max-pooled convolution. For each output map value, they both require computing D^2 inner products followed by finding the maximum response. Epitomic convolution requires D^2 times more work per input patch, but this is exactly compensated by the fact that we extract input patches sparsely with a stride of D pixels.

Similarly to standard max-pooling, the main computational primitive is multi-channel convolution with the set of filters in the epitomic dictionary, which we implement as matrix-matrix multiplication and carry out on the GPU, using the cuBLAS library.

It is noteworthy that conventional max-pooled convolution can be cast as special case of epitomic convolution. More specifically, we can exactly replicate max-pooled convolution with filters of size $W \times W$ and $D \times D$ max-pooling using as epitomes zero-padded versions of the original filters (with padding equal to $D - 1$ pixels on each side of the filter) and epitomic filter size equal to $W + D - 1$. In that sense, epitomic convolution is a generalization of max-pooling.

To build a deep epitomic model, we stack multiple epitomic convolution layers on top of each other. The output of each layer passes through a rectified linear activation unit

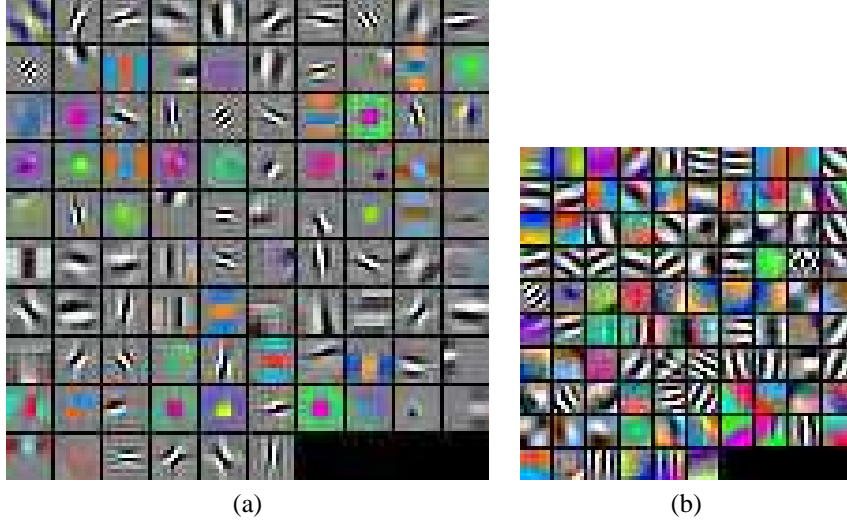


Figure 3. Filters at the first convolutional layer of: (a) Proposed *Epitomic* model with 96 mini-epitomes, each having size 12×12 pixels. (b) Baseline *Max-Pool* model with 96 filters of size 8×8 pixels each.

$y_{i,k} \leftarrow \max(y_{i,k} + \beta_k, 0)$ and fed as input to the subsequent layer, where β_k is the bias. Similarly to [18], the final two layers of our network for Imagenet image classification are fully connected and are regularized by dropout. We learn the model parameters (epitomic weights and biases for each layer) in a supervised fashion by error back propagation. We present full details of our model architecture and training methodology in the experimental section.

2.2. Optional mean and contrast normalization

Motivated by [39], we have explored the effect of filter mean and contrast normalization on deep epitomic network training. More specifically, we considered a variant of the model where the epitomic convolution responses are computed as:

$$(y_{i,k}, p_{i,k}) \leftarrow \max_{p \in \mathcal{N}_{epitome}} \frac{\mathbf{x}_i^T \bar{\mathbf{w}}_{k,p}}{\|\bar{\mathbf{w}}_{k,p}\|_\lambda} \quad (3)$$

where $\bar{\mathbf{w}}_{k,p}$ is a mean-normalized version of the filters and $\|\bar{\mathbf{w}}_{k,p}\|_\lambda \triangleq (\bar{\mathbf{w}}_{k,p}^T \bar{\mathbf{w}}_{k,p} + \lambda)^{1/2}$ is their contrast, with $\lambda = 0.01$ a small positive constant. This normalization requires only a slight modification of the stochastic gradient descent update formula and incurs negligible computational overhead. Note that the contrast normalization explored here is slightly different than the one in [39], who only scale down the filters whenever their contrast exceeds a pre-defined threshold.

We have found the mean and contrast normalization of Eq. (3) to significantly accelerate training not only of epitomic but also max-pooled convolutional nets.

2.3. Image Classification Experiments

Image classification tasks We have performed most of our experimental investigation with epitomes on the Imagenet ILSVRC-2012 dataset [5], focusing on the task of image classification. This dataset contains more than 1.2 million training images, 50,000 validation images, and 100,000 test images. Each image is assigned to one out of 1,000 possible object categories. Performance is evaluated using the top-5 classification error. Such large-scale image datasets have proven so far essential to successfully train big deep neural networks with supervised criteria.

Network architecture and training methodology For our Imagenet experiments, we compare the proposed deep epitomic networks with deep max-pooled convolutional networks. For fair comparison, we use as similar architectures as possible, involving in both cases six convolutional layers, followed by two fully-connected layers and a 1000-way softmax layer. We use rectified linear activation units throughout the network. Similarly to [18], we apply local response normalization (LRN) to the output of the first two convolutional layers and dropout to the output of the two fully-connected layers. This is the Class-A of the models we considered.

The architecture of our baseline *Max-Pool* network is specified on Table 1. It employs max-pooling in the convolutional layers 1, 2, and 6. To accelerate computation, it uses an image stride equal to 2 pixels in the first layer. It has a similar structure with the Overfeat model [32], yet significantly fewer neurons in the convolutional layers 2 to 6. Another difference with [32] is the use of LRN, which to our experience facilitates training.

The architecture of the proposed *Epitomic* network is

Layer	1	2	3	4	5	6	7	8	Out
Type	conv + lrn + max	conv + lrn + max	conv	conv	conv	conv + max	full + dropout	full + dropout	full
Output channels	96	192	256	384	512	512	4096	4096	1000
Filter size	8x8	6x6	3x3	3x3	3x3	3x3	-	-	-
Input stride	2x2	1x1	1x1	1x1	1x1	1x1	-	-	-
Pooling size	3x3	2x2	-	-	-	3x3	-	-	-

Table 1. Architecture of the baseline *Max-Pool* convolutional network (Class-A).

specified on Table 2. It has exactly the same number of neurons at each layer as the *Max-Pool* model but it uses mini-epitomes in place of convolution + max pooling at layers 1, 2, and 6. It uses the same filter sizes with the *Max-Pool* model and the mini-epitome sizes have been selected so as to allow the same extent of translation invariance as the corresponding layers in the baseline model. We use input image stride equal to 4 pixels and further perform epitomic search with stride equal to 2 pixels in the first layer to also accelerate computation.

We have also tried variants of the two models above where we activate the mean and contrast normalization scheme of Section 2.2 in layers 1, 2, and 6 of the network.

We followed the methodology of [18] in training our models. We used stochastic gradient ascent with learning rate initialized to 0.01 and decreased by a factor of 10 each time the validation error stopped improving. We used momentum equal to 0.9 and mini-batches of 128 images. The weight decay factor was equal to 5×10^{-4} . Importantly, weight decay needs to be turned off for the layers that use mean and contrast normalization. Training each of the three models takes two weeks using a single NVIDIA Titan GPU. Similarly to [4], we resized the training images to have small dimension equal to 256 pixels while preserving their aspect ratio and not cropping their large dimension. We also subtracted for each image pixel the global mean RGB color values computed over the whole Imagenet training set. During training, we presented the networks with 220×220 crops randomly sampled from the resized image area, flipped left-to-right with probability 0.5, also injecting global color noise exactly as in [18]. During evaluation, we presented the networks with 10 regularly sampled image crops (center + 4 corners, as well as their left-to-right flipped versions).

Weight visualization We visualize in Figure 3 the layer weights at the first layer of the networks above. The networks learn receptive fields sensitive to edge, blob, texture, and color patterns.

Classification results We report at Table 3 our results on the Imagenet ILSVRC-2012 benchmark, also including re-

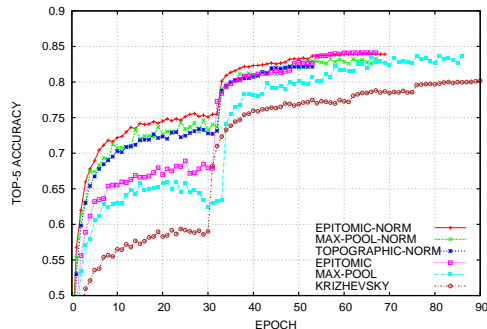


Figure 4. Top-5 validation set accuracy (center non-flipped crop only) for different models and normalization.

sults previously reported in the literature [18, 32, 39]. These all refer to the top-5 error on the validation set and are obtained with a single network. Our best result at 13.6% with the proposed *Epitomic-Norm* network is 0.6% better than the baseline *Max-Pool* result at 14.2% error. The improved performance that we got with the *Max-Pool* baseline network compared to Overfeat [32] is most likely due to our use of LRN and aspect ratio preserving image resizing.

Further experimental results with the epitomic model on the Caltech-101 task and on the MNIST and CIDAR-10 datasets are described in [28].

Mean-contrast normalization and convergence speed

We comment on the learning speed and convergence properties of the different models we experimented with on Imagenet. We show in Figure 4 how the top-5 validation error improves as learning progresses for the different models we tested, with or without mean+contrast normalization. For reference, we also include a corresponding plot we reproduced for the original model of Krizhevsky et al. [18]. We observe that mean+contrast normalization significantly accelerates convergence of both epitomic and max-pooled models, without however significantly influencing the final model quality. The epitomic models converge faster and are stabler during learning compared to the max-pooled baselines, whose performance fluctuates more.

Layer	1	2	3	4	5	6	7	8	Out
Type	epit-conv + lrn	epit-conv + lrn	conv	conv	conv	epit-conv	full + dropout	full + dropout	full
Output channels	96	192	256	384	512	512	4096	4096	1000
Epitome size	12x12	8x8	-	-	-	5x5	-	-	-
Filter size	8x8	6x6	3x3	3x3	3x3	3x3	-	-	-
Input stride	4x4	3x3	1x1	1x1	1x1	3x3	-	-	-
Epitome stride	2x2	1x1	-	-	-	1x1	-	-	-

Table 2. Architecture of the proposed *Epitomic* convolutional network (Class-A).

	Previous literature			Class-A				Class-B	Class-C
Model	Krizhevsky [18]	Zeiler-Fergus [39]	Overfeat [32]	Max-Pool	Max-Pool + norm	Epitomic	Epitomic + norm	Epitomic +norm	Epitomic +norm
Top-5 Error	18.2%	16.0%	14.7%	14.2%	14.4%	13.7%	13.6%	11.9%	10.0%

Table 3. Imagenet ILSVRC-2012 top-5 error on validation set. All performance figures are obtained with a single network, averaging classification probabilities over 10 image crops (center + 4 corners, as well as their left-to-right flipped versions). Classes B and C refer to respectively larger and deeper models.

Experiments with larger and deeper epitomic networks

We have also experimented with larger (Class-B) and very deep (Class-C) versions of the proposed deep epitomic networks. The large Class-B network has the same number of levels but more neurons per layer than the networks in Class-A. It achieves an error rate of 11.9%.

Inspired by the success of the top-performing methods in this year’s Imagenet competition, we have also very recently experimented with a very deep network having 13 convolutional and 3 fully connected layers, which roughly follows the architecture of the 16 layer net in [33]. Our Class-C deep epitomic network achieves 10.0% error rate in the Imagenet task. The state-of-art 16 layer net in [33] (without multi-scale training/testing) achieves an even lower 9.0% error rate, but using a more sophisticated procedure for aggregating the results of multiple image crops (in place of our simple 10-view testing procedure). As extra evidence to the improved robustness of training our deep epitomic networks, it is noteworthy to mention that we managed to train our very deep epitomic net starting from a random initialization, while [33] had to bootstrap their very deep networks from shallower ones.

3. Explicit Scale and Position Search in DCNNs

The effects of object translation and scaling impede the training of accurate classifiers from datasets that lack bounding box annotations - as is the case in the ImageNet classification Challenge. The Epitomic Convolution/Max-Pooling modules allow us to extract an image representation that is invariant to signal deformations taking place at the pooling region’s scale; when used in alternation with feature downsampling (‘striding’) this can result in invariance to increasingly large-scale signal transformations, eventu-

ally dealing with global position and scale changes.

A better treatment of deformations can be achieved by factoring deformations into local (non-rigid) and global (translation/scale) changes. We can then simulate the effect of the latter during training and testing, by transforming the input images, obtaining us an additional hold on the problem. We now describe how this idea can be exploited in the setting of Multiple Instance Learning (MIL).

3.1. MIL-based training of DCNNs

Considering a binary classification problem with N image-label pairs $\mathcal{S} = \{(X_i, y_i), i = 1, \dots, N\}$, training aims at minimizing the following criterion:

$$C(f, \mathcal{S}) = \sum_{i=1}^N l(y_i, f(X_i)) + R(f), \quad (4)$$

where f is the classifier, $l(y, f(X))$ is the loss function and R is a regularizer.

Dataset augmentation amounts to turning an image X_i into a set of images $\mathbf{X}_i = \{X_i^1, \dots, X_i^K\}$ by transforming X_i synthetically; e.g. considering T translations and S scalings yields a set with $K = TS$ elements. The most common approach to using Dataset augmentation consists in treating each element of \mathbf{X}_i as a new training sample, i.e. substituting the loss $l(y, f(X_i))$ in by the sum of the classifier’s loss on all images:

$$L(y_i, \mathbf{X}_i) \doteq \sum_{k=1}^K l(y_i, f(X_i^k)). \quad (5)$$

This corresponds to the dataset augmentation technique use e.g. in [14]. A recently introduced alternative is the ‘sum-pooling’ technique used in [33], which can be understood

as using the following loss:

$$L(y_i, \mathbf{X}_i) = l(y_i, \frac{1}{K} \sum_{k=1}^K f(X_i^k)), \quad (6)$$

which averages the classifier’s score over translated versions of the input image. The summation used in both of these approaches favors classifiers that consistently score highly on positive samples, irrespective of the object’s position and scale - this is when the loss is minimized. As such, these classifiers can be seen as pursuing the invariance of f .

There is however a tradeoff between invariance and classification accuracy [36]. Even though pursuing invariance accounts for the effects of transformations, it does not make the classification task any easier: the training objective aims at a classifier that would allow all transformed images to make it through its ‘sieve’. Understandably, a classifier that only considers centered objects of a fixed scale can achieve higher accuracy: this would allow us to devote all modelling resources to the treatment of local deformations.

For this, we let our classifier ‘choose’ its preferred transformation. In particular, we define the loss function to be:

$$L(y_i, \mathbf{X}_i) = l(y_i, \max_k f(X_i^k)), \quad (7)$$

which amounts to letting the classifier choose the transformation that maximizes its response on a per-sample basis, and then accordingly penalizing that response. In particular the loss function requires that the classifier’s response is large on at least one position for a positive sample - and small everywhere for a negative.

This idea amounts to the simplest case of Multiple Instance Learning [6]: \mathbf{X}_i can be seen as a *bag of features* and the individual elements of \mathbf{X}_i can be seen as *instances*. For the particular case of the hinge loss function, this would lead us to the latent-SVM training objective [2, 8].

Using this loss function during training amounts to treating the object’s position and scale as a latent variable, and performing alternating optimization over the classifier’s score function. During testing we perform a search over transformations and keep the best classifier score, which can be understood as maximizing over the latent transformation variables. The resulting score $F(\mathbf{X}_i) = \max_k f(X_i^k)$ is transformation-invariant, but is built on top of a classifier tuned for a single scale- and translation- combination. The MIL setting allows us to train and test our classifiers consistently, using the same set of image translations and scalings.

3.2. Efficient Convolutional Implementation

We now turn to practical aspects of integrating MIL into DCNN training. DCNNs are commonly trained with input images of a fixed size, $q \times q$. For an arbitrarily-sized input image I , if we denote by $\mathcal{I}(x, y, s)$ its image pyramid, naively computing the maximization in Eq. 7 would

Model	Epitomic (Class-B)	Epitomic (patchwork)
Top-5 Error	11.9%	10.0%

Table 4. Imagenet ILSVRC-2012 top-5 error on validation set. We compare the Class-B mean and contrast normalized deep epitomic network of Table 3 with its Patchwork fine-tuned version that also includes scale and position search.

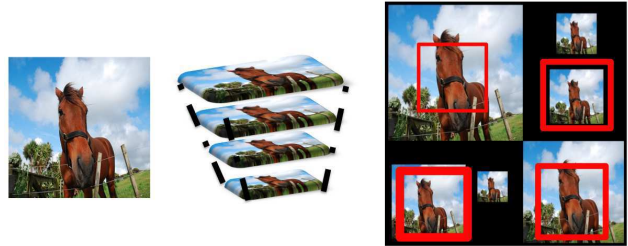


Figure 5. We use the image patchwork technique to efficiently implement scale and position search in DCNN training: an image pyramid is unfolded into a image ‘patchwork’, where sliding a fixed-size window amounts to search over multiple positions and scales. The maximum of the classifier’s score on all such windows is efficiently gathered by max-pooling the DCNN’s top-layer responses, and is used to accommodate scale and position changes during both training and testing.

require to cropping many $q \times q$ boxes from $\mathcal{I}(x, y, s)$, evaluating f on them, yielding $f(x, y, s)$, and then penalizing $l(y, \max_{x, y, s} f(x, y, s))$ during training (we ignore down-sampling and boundary effects for simplicity). Doing this would require a large amount of GPU memory, communication and computation time. Instead, by properly modifying the input and architecture of our network we can share computation to efficiently implement exhaustive search during training and testing.

For this, we first draw inspiration from the ‘image patchwork’ technique introduced in [7] and exploited in DCNNs by [10]. The technique consists in embedding a whole image pyramid $\mathcal{I}(x, y, s)$, into a single, larger, patchwork image $P(x', y')$; any position (x', y') in P corresponds to a (x, y, s) combination in I . This was originally conceived as a means of accelerating multi-scale FFT-based convolutions in [7] and convolutional feature extraction in [10]. Instead we view it a stepping stone to implementing scale and position search during DCNN training.

In particular, we treat the last, fully-connected, layers of a DCNN as 1×1 convolution kernels; we can then obtain the $f(x, y, s)$ score described above by providing P as input to our network, since the output of our network’s final layer at any position (x', y') will correspond to the output corresponding to a $q \times q$ square cropped around (x, y, s) . This allows us to incorporate the max operation used in MIL’s training criterion, Eq. 7, as an additional max-pooling layer situated on top of the network’s original score function.

This makes it possible to efficiently incorporate global scale and position search in a seamless manner within DCNN training.

3.3. Image Classification Results

We have experimented with the scheme outlined above in combination with our Deep Epitomic Network (Class-B variant) presented in the previous Section. We use a 720×720 patchwork formed from 6 different image scales (square boxes with size 400, 300, 220, 160, 120, and 90 pixels). We have resized all train/test images to square size, changing their aspect ratio if needed. We have initialized this scale/position search net with the parameters of our standard Class-B epitomic net. We fine-tuned the network parameters for about an epoch on the Imagenet train set, following the training methodology outlined earlier.

We have obtained a substantial further decrease in the testing error rates, cutting the top-5 error rate from 11.9% down to 10.0%, as shown in Table 4. This reduction in error rate is competitive with the best reduction obtained by more complicated techniques involving many views for evaluation [33, 33], while also allowing for consistent end-to-end training and testing.

The network outlined above also provides cues for the scale and position of the dominant object in the image. A simple fixed mapping of the “argmax” patchwork position in the last max-pooling layer (computed by averaging the bounding box positions in the training set) yields 48.3% error rate in the Imagenet 2012 localization task without incurring any extra computation.

4. Sliding Window Object Detection with DCNNs

The success of explicit position and scale search in image classification suggests using DCNNs for sliding-window detection; even though for pedestrians excellent results have been reported in [25] recent works on combining convolutional networks [32], or sliding window detectors with CNN features [10, 27] still lag behind the current state-of-the-art techniques [9, 13, 24].

Starting from the RCNN work of [9], all such techniques compute DCNN features ‘on-demand’ for a set of 1000-2000 image regions delivered by selective search [35], and apply a separately trained SVM detection on top. This approach has recently been shown to deliver compelling detection results; most recently, [9] have shown that combining RCNNs with the network of [33] pushes the mean AP performance on Pascal VOC 2007 to 66% (62% without bounding box regression), but at the cost of 60 seconds per image (acceleration techniques such as Spatial Pyramid Pooling [13] can still be applied, though).

Despite the performance gap of sliding window detection to RCNNs, we consider sliding window detection sim-

pler, and potentially more amenable to analysis and improvement.

4.1. Explicit search over aspect ratios

Our basic object detection system uses as input to a DCNN an image patchwork that includes 11 scales logarithmically sampled, from 2 times down to 1/6 of the image size. Unlike recent works [10, 27] that only operate with the first five, ‘convolutional’ layers of a deeper network, in our case we set the fully-connected layers operate convolutionally, and use the DCNN class scores for proposing square bounding boxes as object detection proposals. This processes a typical PASCAL VOC 2007 image in less than 1 sec on a Titan Tesla K40.

This square bounding box detector (without any bounding box regression post-processing) yields a mean Average Precision of 43.0% on Pascal VOC 2007. To further analyze which of this system’s errors are due to constraining the bounding box proposals to be square, we investigated the system’s performance in the presence of an ‘oracle’ that provides the optimal aspect ratio (using the ground truth annotations) for any given square bounding box proposal. We found this oracle bounding box prediction to increase performance to 56.7%. This indicates that square box prediction is insufficient for achieving competitive object detection results.

Once again, we pursue an explicit search approach to directly estimate the aspect ratio of bounding box proposals without needing to resort to an oracle. We account for aspect ratio variability by scaling the image along a single dimension. For instance, scaling an image by .5 vertically means that a vertically-elongated 100×200 region appears as a 100×100 square region in the transformed image. Our square detector can then find this preferable to other, differently scaled versions of the same region, and thereby hint at the right object ratio. Aspect ratios that receive a lower score are eliminated at the final nonmaximum suppression stage. We account for aspect ratio during both testing and training (see below).

We perform this operation for 5 distinct aspect ratios, spanning the range of $[1/3, 3]$ with a geometric progression, as illustrated in Figure 6. This is applied at the whole patchwork level – sliding window detection on these patchworks then amounts to a joint search over scale, position, and aspect ratio. This is more time-demanding (requiring 5 times more computation) but still quite fast, requiring about 5 secs on a Tesla K40 for an average Pascal VOC 2007 image, and yields non-square bounding box predictions without resorting to an oracle.

The related detection results are shown in Table 5. Aspect ratio search yields a very competitive mean Average Precision score of 56.4% (without any bounding box regression post-processing). This is only slightly lower than the

oracle-based score 56.7%, indicating that also normalizing for aspect ratio during training leads to better object models.

It is noteworthy that our 56.4% mAP result is significantly better than the 46.9% mAP result reported very recently by [37]. Our better results should be attributed to our different training procedure (detailed below), our explicit search over aspect ratios, and the use of a more powerful DCNN classifier. Our system is also significantly simpler than [37] (which also integrates deformable part models and includes non maximum suppression during training). We anticipate that integrating these components into our system could further increase performance at a higher computational cost.

We observe that our system’s average performance (56.4% mAP) is still below the one obtained by [9] when using the network of [33] (62.2% mAP without bounding box regression). This can be attributed to several aspects of our system, including (i) using a smaller number of network parameters (detailed below) (ii) performing the detection with smaller windows (detailed below) (iii) not using a retraining stage with the hinge loss and hard-negative mining, as [9] do, and (iv) missing out on regions found by Selective Search. We are confident that factor (iv) is the least important - having experimentally verified that the recall of bounding boxes is systematically better according to our pyramid’s hypothesized positions, rather than the boxes delivered by Selective Search. We are currently investigating the effects of factors (i)-(iii). Still, we consider that our system has an edge on the efficiency side: our detector requires approximately 5 seconds to consider all position, scale and aspect ratio combinations, while the system of [9] with the network of [33] requires approximately 60 seconds, on identical hardware (a Tesla K40 GPU).

4.2. DCNN training for sliding window detection

We deviate from the network fine-tuning used in the RCNN system [9] in two ways: firstly, we do not rely on the Selective Search [35] region proposals to gather training samples; and, secondly, we modify the network’s structure to process smaller images, and, resultantly, include less parameters. We detail these two modifications below.

4.2.1 Model Training

The RCNN system of [9] adapts a network trained for the Imagenet classification task to object detection on Pascal VOC. For this, the authors use the regions proposed by selective search to generate positive and negative training samples, for each of the 20 categories of Pascal VOC; if a region has an Intersection-over-Union (IoU) above .5 for any bounding box of a class it is declared as being a positive example for that class, or else it is a negative example. These examples are used in a network ‘fine-tuning’

stage, which amounts to running back-propagation with these training samples.

Rather than relying on Selective Search to provide training samples, we exploit the dense sampling of positions, scales, and aspect ratios of our algorithm. This allows us to use substantially cleaner examples, and train with a higher IoU threshold for positives.

In particular, as illustrated in Figure 7, we keep track of all the windows that would be visited by our sliding window detector; given a ground-truth bounding box, we randomly pick 30 of those that have an IoU score above 0.7 with it; if we have less than 30, we decrease the threshold to 0.6 and if we still cannot find as many we set the threshold finally to 0.5. Similarly, for every positive bounding box we sample 200 negative boxes that have an IoU score between 0.2 and 0.5 - aiming at ‘teaching’ our classifier what a poor localization looks like.

We have verified that doing this, rather than using selective search windows gives us clearly better detector scores, both visually and quantitatively. We consider this to be one of the advantages of using a sliding window detector, namely that we do not need to rely on an external region proposal module for training.

4.2.2 Re-purposing Classification Networks for Image Detection

Herein we describe how we have re-purposed the publicly available state-of-art 16 layer classification network of [33] (VGG-16) into an efficient and effective component of our sliding window detector.

Dense sliding window feature extraction with the hole algorithm Dense spatial score evaluation is instrumental in the success of our CNN sliding window detector.

As a first step to implement this, we convert the fully-connected layers of VGG-16 into convolutional ones and run the network in a convolutional fashion on the patchwork. However this is not enough as it yields very sparsely computed detection scores (with a stride of 32 pixels). To compute scores more densely at our target stride of 8 pixels, we develop a variation of the method previously employed by [11, 32]. We skip subsampling after the last two max-pooling layers in the network of [33] and modify the convolutional filters in the layers that follow them by introducing zeros to increase their length (2× in the last three convolutional layers and 4× in the first fully connected layer). We can implement this more efficiently by keeping the filters intact and instead sparsely sample the feature maps on which they are applied on using a stride of 2 or 4 pixels, respectively. This approach is known as the ‘hole algorithm’ (‘trous algorithm’) and has been developed before for efficient computation of the undecimated wavelet

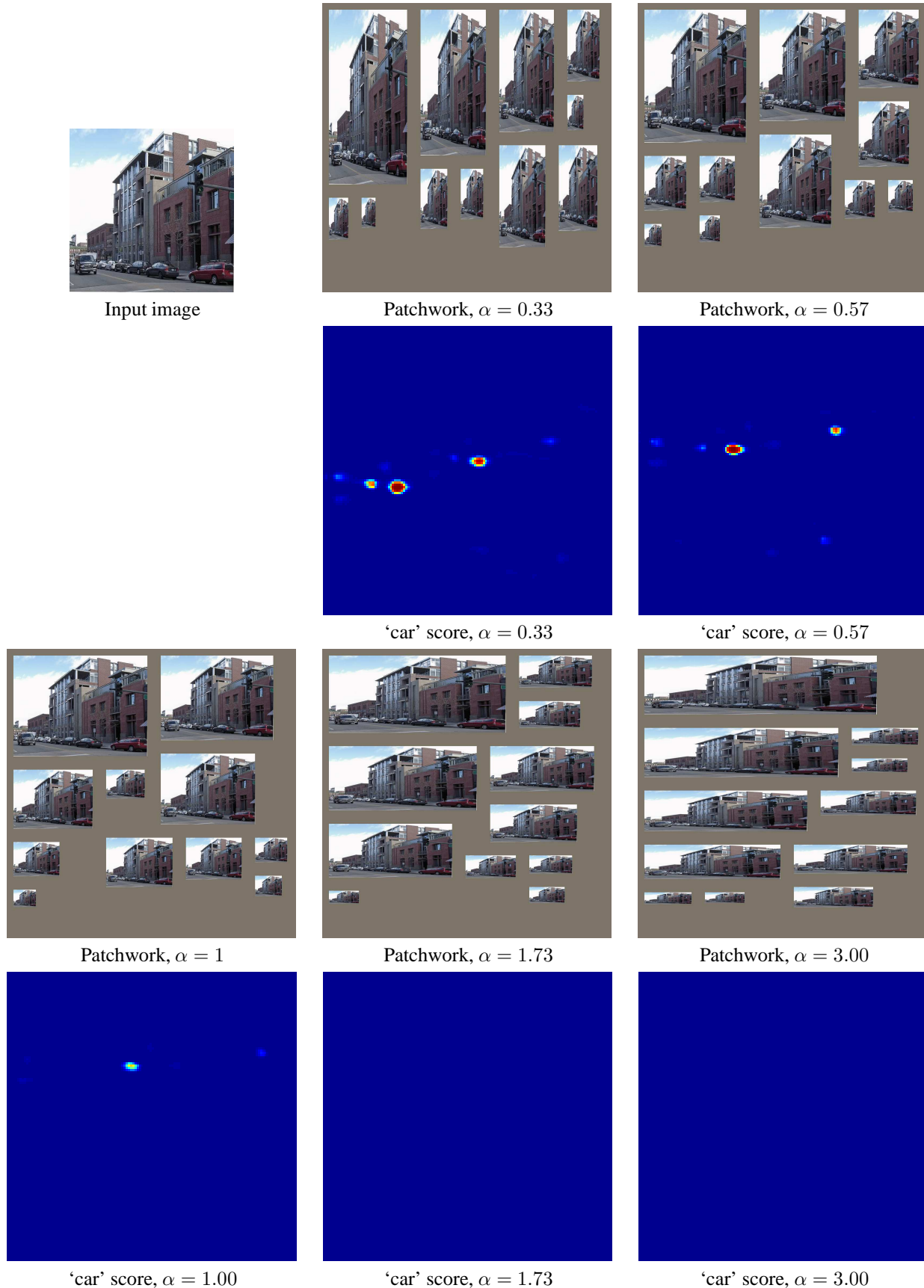


Figure 6. Patchwork images (even rows) and car detector scores (odd rows) used for explicit position, scale, and aspect ratio (*alpha*) search. We observe that the score is maximized at patchwork positions (i.e. image positions, scale, and aspect ratio combinations) corresponding to square-shaped cars.

VOC 2007 test	aero	bike	bird	boat	bottle	bus	car	cat	chair	cow	table	dog	horse	mbike	person	plant	sheep	sofa	train	tv	mAP
Our work (VGG)	64.4	72.1	54.6	40.4	46.5	66.2	72.9	58.2	31.8	69.8	31.8	59.3	71.1	68.3	64.7	31.0	55.0	49.8	55.3	64.4	56.4
RCNN7 [9] (VGG)	71.6	73.5	58.1	42.2	39.4	70.7	76.0	74.5	38.7	71.0	56.9	74.5	67.9	69.6	59.3	35.7	62.1	64.0	66.5	71.2	62.2
RCNN7 [9] (UoT)	64.2	69.7	50.0	41.9	32.0	62.6	71.0	60.7	32.7	58.5	46.5	56.1	60.6	66.8	54.2	31.5	52.8	48.9	57.9	64.7	54.2
DPM [37] (UoT)	49.3	69.5	31.9	28.7	40.4	61.5	61.5	41.5	25.5	44.5	47.8	32.0	67.5	61.8	46.7	25.9	40.5	46.0	57.1	58.2	46.9

Table 5. Detection average precision (%) on the PASCAL VOC 2007 test set, using the proposed CNN sliding window detector that performs explicit position, scale, and aspect ratio search. We compare to the RCNN architecture of [9] and the end-to-end trained DPMs of [37]. In parenthesis we indicate the DCNN used for detection: UoT is the University of Toronto DCNN [18] and VGG is the DCNN of Oxford’s Visual Geometry Group [33].



Sliding window positives (left) and negatives (right)

Selective search positives (left) and negatives (right).

Figure 7. Bounding boxes used for network finetuning. Our sliding window detector can use many more bounding boxes as positives (a) and negatives (b). The training samples available from selective search (c) are fewer, forcing the training to use poorly localized positives (d). When finetuning our network only with the latter examples performance would deteriorate.

transform [23]. We have implemented this within the Caffe framework by adding to the *im2col* function (it converts multi-channel feature maps to vectorized patches) the option to sparsely sample the underlying feature map.

Shrinking the receptive field of neural networks Most recent DCNN-based image recognition methods rely on networks pre-trained on the Imagenet large-scale classification task. These networks typically have large receptive field size, 224×224 in the case of the VGG-16 net we consider. We have found this receptive field size to be too large to allow good localization accuracy (unless one uses heavily zoomed-in versions of the image). Moreover, after converting the network to a fully convolutional one, the first fully connected layer has 4,096 filters of large 7×7 spatial size and becomes the computational bottleneck in our sliding window detector system.

We have addressed both of these serious practical problems by spatially subsampling the first FC layer to 4×4 spatial size. This has reduced the receptive field of the network down to 128×128 pixels and has reduced computation time for the first FC layer by 3 times.

5. Conclusions

This paper examines multiple facets of invariance in the context of deep convolutional networks for visual recognition. First, we have proposed a new epitomic convolutional layer which acts as a substitute to a pair of consecutive convolution and max-pooling layers, and shown that

it brings performance improvements and exhibits better behavior during training. Second, we have demonstrated that treating scale and position as latent variables and optimizing over them during both training and testing yields significant image classification performance gains. Pushing scale and position search further, we have shown promising results which suggest that DCNNs can be efficient and effective for dense sliding window based object detection. Further pursuing this topic is the main direction of our future work.

Reproducibility We implemented the proposed methods by extending the excellent Caffe software framework [16]. When this work gets published we will publicly share our source code and configuration files with exact parameters fully reproducing the results reported in this paper.

Acknowledgments We gratefully acknowledge the support of NVIDIA Corporation with the donation of GPUs used for this research.

References

- [1] M. Aharon and M. Elad. Sparse and redundant modeling of image content using an image-signature-dictionary. *SIAM J. Imaging Sci.*, 1(3):228–247, 2008. 2
- [2] S. Andrews, T. Hofmann, and I. Tsochantaridis. Support vector machines for multiple instance learning. In *NIPS*, 2002. 7

- [3] L. Benoit, J. Mairal, F. Bach, and J. Ponce. Sparse image representation with epitomes. In *Proc. CVPR*, pages 2913–2920, 2011. [2](#)
- [4] K. Chatfield, K. Simonyan, A. Vedaldi, and A. Zisserman. Return of the devil in the details: Delving deep into convolutional nets. *arXiv*, 2014. [1](#), [5](#)
- [5] J. Deng, W. Dong, R. Socher, L. Li-Jia, K. Li, and L. Fei-Fei. Imagenet: A large-scale hierarchical image database. In *Proc. CVPR*, 2009. [1](#), [4](#)
- [6] T. G. Dietterich, R. H. Lathrop, and T. Lozano-perez. Solving the multiple-instance problem with axis-parallel rectangles. *Artificial Intelligence*, 89:31–71, 1997. [7](#)
- [7] C. Dubout and F. Fleuret. Exact acceleration of linear object detectors. In *Computer Vision–ECCV 2012*, pages 301–311. Springer Berlin Heidelberg, 2012. [7](#)
- [8] P. Felzenszwalb, R. Girshick, D. McAllester, and D. Ramanan. Object detection with discriminatively trained part-based models. *IEEE Trans. PAMI*, 32(9):1627–1645, 2010. [7](#)
- [9] R. Girshick, J. Donahue, T. Darrell, and J. Malik. Rich feature hierarchies for accurate object detection and semantic segmentation. In *Proc. CVPR*, 2014. [1](#), [8](#), [9](#), [11](#)
- [10] R. Girshick, F. Iandola, T. Darrell, and J. Malik. Deformable part models are convolutional neural networks. *arXiv preprint arXiv:1409.5403*, 2014. [7](#), [8](#)
- [11] A. Giusti, D. Ciresan, J. Masci, L. Gambardella, and J. Schmidhuber. Fast image scanning with deep max-pooling convolutional neural networks. In *Proc. IEEE Int. Conf. on Image Processing*, 2013. [9](#)
- [12] I. Goodfellow, D. Warde-Farley, M. Mirza, A. Courville, and Y. Bengio. Maxout networks. In *Proc. ICML*, 2013. [2](#), [3](#)
- [13] K. He, X. Zhang, S. Ren, and J. Sun. Spatial pyramid pooling in deep convolutional networks for visual recognition. In *ECCV*, 2014. [8](#)
- [14] A. G. Howard. Some improvements on deep convolutional neural network based image classification, 2013. *arXiv:1409.0575*. [6](#)
- [15] K. Jarrett, K. Kavukcuoglu, M. Ranzato, and Y. LeCun. What is the best multi-stage architecture for object recognition? In *Proc. ICCV*, pages 2146–2153, 2009. [1](#)
- [16] Y. Jia. Caffe: An open source convolutional architecture for fast feature embedding, 2013. [11](#)
- [17] N. Jojic, B. Frey, and A. Kannan. Epitomic analysis of appearance and shape. In *Proc. ICCV*, pages 34–41, 2003. [2](#)
- [18] A. Krizhevsky, I. Sutskever, and G. Hinton. ImageNet classification with deep convolutional neural networks. In *Proc. NIPS*, 2013. [1](#), [2](#), [3](#), [4](#), [5](#), [6](#), [11](#)
- [19] Y. LeCun, L. Bottou, Y. Bengio, and P. Haffner. Gradient-based learning applied to document recognition. *Proc. IEEE*, 86(11):2278–2324, 1998. [1](#)
- [20] H. Lee, R. Grosse, R. Ranganath, and A. Y. Ng. Convolutional deep belief networks for scalable unsupervised learning of hierarchical representations. In *Proc. ICML*, 2009. [3](#)
- [21] M. Lin, Q. Chen, and S. Yan. Network in network. In *ICLR*, 2014. [1](#)
- [22] D. Lowe. Distinctive image features from scale-invariant keypoints. *IJCV*, 60(2):91–110, 2004. [1](#)
- [23] S. Mallat. *A Wavelet Tour of Signal Processing*. Acad. Press, 2 edition, 1999. [11](#)
- [24] W. Ouyang, P. Luo, X. Zeng, S. Qiu, Y. Tian, H. Li, S. Yang, Z. Wang, Y. Xiong, C. Qian, Z. Zhu, R. Wang, C. C. Loy, X. Wang, and X. Tang. Deepid-net: multi-stage and deformable deep convolutional neural networks for object detection. *CoRR*, abs/1409.3505, 2014. [8](#)
- [25] W. Ouyang and X. Wang. Joint deep learning for pedestrian detection. In *ICCV*. [8](#)
- [26] W. Ouyang and X. Wang. Joint deep learning for pedestrian detection. In *Proc. ICCV*, 2013. [1](#)
- [27] P.-A. Savalle and S. Tsogkas and G. Papandreou and I. Kokkinos. Deformable part models with cnn features. In *3rd Parts and Attributes Workshop, ECCV*. [8](#)
- [28] G. Papandreou. Deep epitomic convolutional neural networks. *arXiv*, 2014. [2](#), [5](#)
- [29] G. Papandreou, L.-C. Chen, and A. Yuille. Modeling image patches with a generic dictionary of mini-epitomes. In *Proc. CVPR*, 2014. [2](#)
- [30] A. Razavian, H. Azizpour, J. Sullivan, and S. Carlsson. CNN features off-the-shelf: An astounding baseline for recognition. In *Proc. CVPR Workshop*, 2014. [1](#)
- [31] M. Riesenhuber and T. Poggio. Hierarchical models of object recognition in cortex. *Nature neuroscience*, 2(11):1019–1025, 1999. [1](#)
- [32] P. Sermanet, D. Eigen, X. Zhang, M. Mathieu, R. Fergus, and Y. LeCun. Overfeat: Integrated recognition, localization and detection using convolutional networks. 2014. [1](#), [2](#), [4](#), [5](#), [6](#), [8](#), [9](#)
- [33] K. Simonyan and A. Zisserman. Very deep convolutional networks for large-scale image recognition, 2014. <http://arxiv.org/abs/1409.1556/>. [1](#), [2](#), [6](#), [8](#), [9](#), [11](#)

- [34] C. Szegedy, W. Liu, Y. Jia, P. Sermanet, S. Reed, D. Anguelov, D. Erhan, V. Vanhoucke, and A. Rabinovich. Going deeper with convolutions. *CoRR*, abs/1409.4842, 2014. [1](#)
- [35] J. R. R. Uijlings, K. E. A. van de Sande, T. Gevers, and A. W. M. Smeulders. Selective search for object recognition. 2013. [8](#), [9](#)
- [36] M. Varma and D. Ray. Learning the discriminative power-invariance trade-off. In *ICCV*, 2007. [7](#)
- [37] L. Wan, D. Eigen, and R. Fergus. End-to-end integration of a convolutional network, deformable parts model and non-maximum suppression. *arXiv*, 2014. [9](#), [11](#)
- [38] M. Zeiler and R. Fergus. Stochastic pooling for regularization of deep convolutional neural networks. 2013. [3](#)
- [39] M. Zeiler and R. Fergus. Visualizing and understanding convolutional networks. *arXiv*, 2013. [1](#), [2](#), [4](#), [5](#), [6](#)
- [40] M. Zeiler, D. Krishnan, G. Taylor, and R. Fergus. Deconvolutional networks. In *Proc. CVPR*, 2010. [3](#)